**APB manuscript No.**
(will be inserted by the editor)

# Phase sensitive radial extraction and mass spectrometry of trapped ions in a compact geometry

**S. Jyothi, Tridib Ray and S. A. Rangwala**

Raman Research Institute, Bangalore 560080, India

July 15, 2014

**Abstract** The detection of trapped atomic and molecular ions of Rubidium, by extraction, from our thin-wire electrode modified spherical Paul trap, is discussed in detail. The compact geometry poses serious challenges and constraints for efficient extraction and reliable detection of ions. The solution to the dual challenge of counting the trapped ions with minimum pile up loss as well as detection that permits reliable mass spectroscopy is experimentally implemented. The details of the ion extraction process are understood by numerical simulation. The experimental and numerical data are compared and found to be in close agreement. The reliability of the technique for future, multi species experiments, is established and possible improvements are discussed.

## 1 Introduction

Advances in studies of ultracold dilute gas mixtures in recent times have led to the development of variety of hybrid traps, where mixtures are studied. Trapped ion-atom mixtures have been at the center of much activity, and diverse technical implementations for studing these mixtures have been implemented [1–7]. Modern ion trap experiments range from experiments with trapped mixtures, precision measurements [8], quantum information processing [9] and condensed matter physics [10]. Such experiments have led to substantial innovation in the construction of new ion trap configurations, suited for specific science goals.

The experimental system presented here consists of an ion-atom hybrid trap assembly built within a Fabry-Perot cavity [11,12]. The position of the cavity with respect to the trap geometry requires that the ion extraction from the trap is not along the highest symmetry axis, but along the axis of lower symmetry transverse to the axis of the ion trap. To enable ion extraction, appropriate voltages on a set of electrodes are turned on, to provide an electric field gradient which pushes the trapped ions onto a channel electron multiplier (CEM). The ion extraction to the CEM can be performed even while the trapping potential is on. In this case however, the arrival time distribution of the ions is found to be critically dependant on the phase of the radio frequency (rf) potential at which the extraction voltages are switched on [13,14]. Here we report our results for the radial extraction of ions. The radial extraction of ions from a spherical Paul trap with the trapping rf voltage on and its consequences are demonstrated for the first time. This is significantly different from the radial extraction from a linear Paul trap for mass spectrometry [15], in which case the rf trapping field is switched off before extraction. A combination of experiments and numerical simulations to understand the consequences of radial extraction are presented in detail. We show that when a single ion species is present, phase sensitive extraction is very effective at reducing the count pile-up problem by spreading the ion signal. On the other hand when multiple species of ions are present, the resolved mass spectra are obtained when the rf is switched off during ion extraction from the trap. A combination of both strategies gives all the flexibility required to study trapped ion atom mixtures.

## 2 The ion trap

The ion trap discussed here [11] is a modified spherical Paul trap consisting of four Tungsten wire loops wound in square geometry over groved ceramic sleeves jacketing four stainless steel (SS316) rods. The basic structure of the experiment is illustrated in Fig. 1. The rods are 3 mm in diameter and are arranged in a quadrupole geometry with a center to center distance of 17 mm. The Tungsten wire is 80 $\mu$m in diameter and the wound loops are separated by 1.5 mm, 3 mm and 1.5 mm respectively. Each rod and wire loop is electrically isolated by the ceramic sleeves and can therefore be independently biased. The ion trap secular potential is obtained by applying appropriate radio frequency voltage on the inner pair of wires. A small dc voltage on the outer two wires can be used to change the trap depth in the radial and axial directions [11].

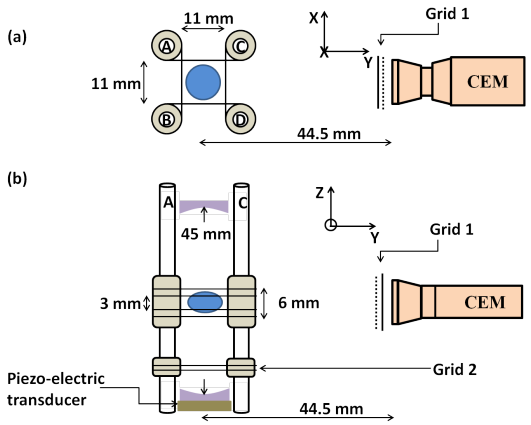


Fig. 1: (a) and (b) represents the axial and top view of the four wire ion trap. The wires are wound on the grooves made on a ceramic which are fixed on four quadrupole rods A, B, C and D. The blue sphere and ellipsoid represents the maximal spatial extent for a trapped rubidium ion, with the operating parameters reported in the text. The trapped ions are extracted onto the CEM using the extraction voltages described in the text. One set of two grids, screens the CEM cone voltage from the trap volume, while another grid set along the trap axis corrects for the bias potential on the piezoelectric transducer attached to one of the cavity mirrors.

The potential due to all the electrodes in the experiment and metallic surfaces at ground potential, including the chamber are generated using SIMION$^{TM}$. Stable operating parameters for the ion trap are determined by by solving the coupled differential equations of motion for the ions, in this potential. The ion trap is characterized experimentally and numerically for $^{85}Rb^{+}$ and $^{85}Rb_2^{+}$ions.

The atomic ions are created by 2 photon ionization from Rb atoms in a magneto optical trap (MOT). The cooling laser of the MOT excites the atom to the first excited 5p state, and these excited atoms are ionized by the application of a short pulse of 473 nm laser. The operating conditions for the ion trap are decided experimentally by optimizing on a combination of rf voltage at a convenient frequency of trap operation, end cap voltage and for trapped ion lifetime. The optimal rf voltage on the inner wire pair is found to be $V_{rf} = 80$ V at 500kHz with a dc voltage of -5V on the outer pair of wires. Results of simulations for optimal trap parameters are in good agreement with the experimental values for trap operation [11].

To study trapped molecular ions interacting with a cold dilute gas of trapped atoms requires that the molecular ions be reliably detected when atomic ions are co-trapped. The optimized parameters for $Rb^{+}$ ion trapping are unsuitable for stable trapping of $Rb_2^{+}$ ions, as is illustrated in Fig. 2. For mass spectrometry of ions in radial extraction for a compact geometry we create both the $Rb^{+}$ and $Rb_2^{+}$ ions by the same method and at the same time. Working with a small number of trapped $Rb^{+}$ and

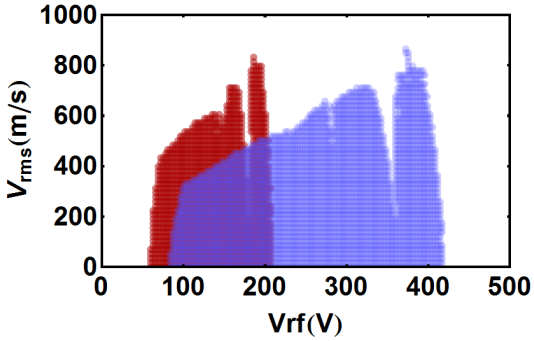


Fig. 2: Here we show the maximum initial rms velocity that an ion at the centre can have to be trapped for an applied voltage, as a function of $V_{rf}$ at 500 kHz. The red and blue circles represents the $Rb^{+}$ and $Rb_2^{+}$ ions respectively. Clearly, while the trap regions of $Rb^{+}$ and $Rb_2^{+}$ overlap, the best point for simultaneous trapping is between individual optimal frequencies.

$Rb_2^{+}$ ions ensures that there are no space charge effects which are folded into the mass spectrum. Low ion numbers are also desirable to avoid the effect of detector pile-up and to validate the experimental technique for reliable ion counting and mass spectrometry with low ion numbers. In this experiment, $Rb^{+}$ and $Rb_2^{+}$ ions are simultaneously created from the MOT atoms using a pulsed dye laser (wavelength set to 602.6 nm, pulse duration 1-2 ns) pumped by the second harmonic of a Nd:YAG laser (10 Hz repetition rate). The $Rb^{+}$ ions are formed by three photon ionization of the ground state Rb atoms in the MOT by the dye laser pulse. Cold $Rb_2$ molecules are spontaneously formed in the MOT by long range photo association of the atoms in the presence of the cooling laser light. A fraction of the photo associated molecules decay to vibrational levels of the ground electronic molecular state. These ground state molecules are then ionized to a vibrational distribution of $Rb_2^{+}$ molecular ion states by two photon transition by the dye laser pulse at 602.6 nm [16, 17]. In this manner both the atomic and molecular ions of $Rb_2^{+}$ are created, and each pules of the dye laser creates only a few ions. Both the species of ions are held in the ion trap for 300 $\mu$s after the ionizing pulse and then extracted. The ion trap rf voltage is set to 130 V in this case to simultaneously trap both the species of ions.

## 3 Trapped Ion Extraction

The trapped ions are detected by extracting them onto a CEM mounted perpendicular to the stainless steel rods, with the CEM cone at a distance of 44.5 mm from the ion trap center. The CEM is maintained at a high voltage of $-2.4$ kV. A dual grid mesh arrangement facing the ion trap and a grounded metal housing around the CEM ensures that the CEM voltages do not affect ion trap operation. The ions are extracted from the trap to

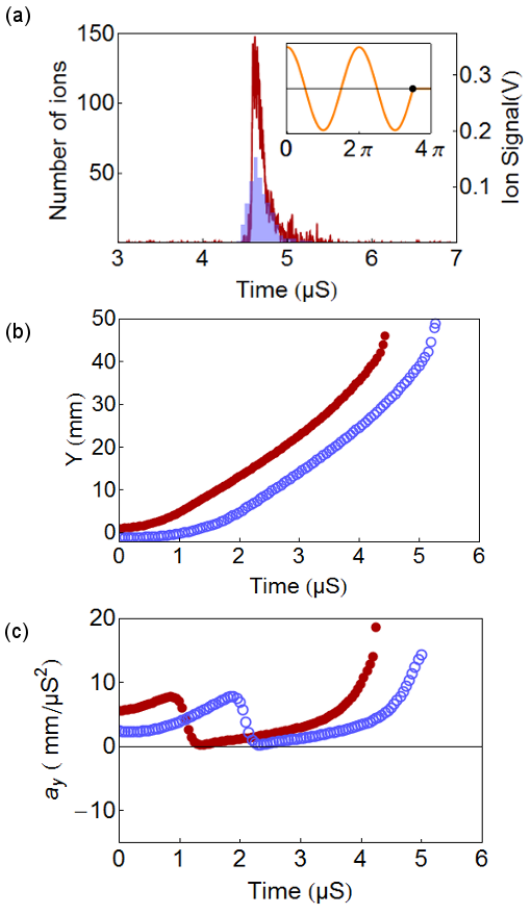


Fig. 3: (a) The ToF signal of $Rb^+$ ions extracted when the rf voltage is switched off and extraction voltages are switched on simultaneously, when the amplitude of the rf voltage is zero. The red curve is the experimental signal and the blue histogram is the result of simulation. The ordinate axis on the left represents the ion number for the simulation and the right ordinate is the integrated ion signal. This convention holds all through the manuscript and the values on the two ordinates scales are independent. (b) Shows the extracted ion's trajectory from the ion trap towards the CEM. The red (thick) and blue (open) circles represents the trajectory of those ions at the two extremes of the ToF signal. The acceleration these ions have experienced as a function of time during their time of flight is shown (c).

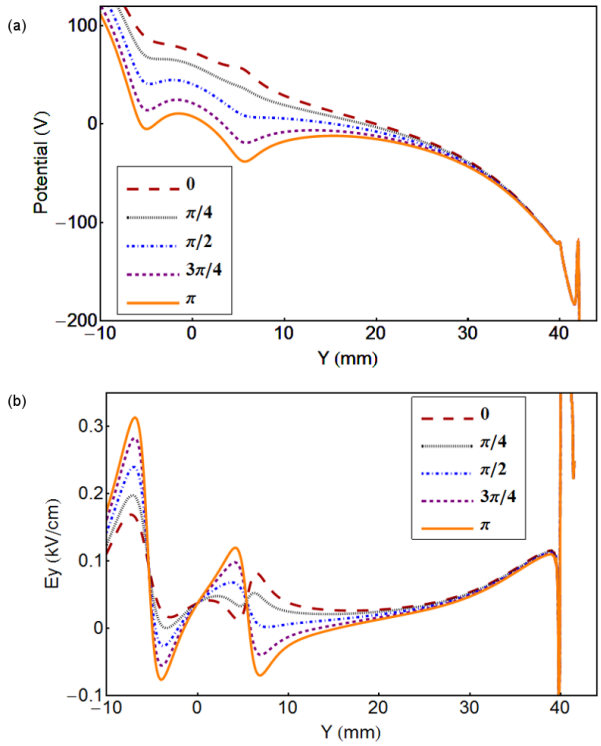


Fig. 4: (a) and (b) shows the potential and electric field respectively, in the extraction axis at different phases of the trapping rf field. The curves are plotted in different line styles and colors and corresponds to the phase points in the inset. The voltages on the extraction electrodes are as described in the text.

the CEM, by switching a high extraction voltage ($V_e$) of 400 V on electrodes A and B (Fig. 1), while maintaining electrodes C and D at ground potential. The CEM grid is switched from ground to −120 V at the same time. As shown in the Fig. 1, an additional pair of tungsten wires are wound in front of one of the cavity mirrors, which is attached to a piezo electric transducer(PZT). This electrode is grounded when trap is operational to shield the trap centre from any voltage applied on the PZT and switched to ≈ 100 V during extraction to provide a symmetric extraction electric field. For effective single shot extraction, it is important that the extraction voltage is significantly larger than the rf voltage, so that all the ions can exit the trapping potential. While the presence of the ceramic sleeves can be expected to modify the extraction field, in a manner that cannot be quantified numerically, the resulting change is small as bourn out by the experimental measurements presented below and their close agreement with the numerical simulations of the ion extraction.

Ion extraction can be performed with rf ON or rf OFF on the innerwires of the modified spherical Paul trap. To understand the extracted ion distribution in these two cases, a set of experiments at different extraction phases are performed and compared with the corresponding numerical simulations. Below we first discuss the consquences of ion extraction in the two cases when only the atomic ion of $Rb^+$ is created and trapped in the ion trap.

### *3.1 Atomic Ion: Extraction with rf OFF*

The ion extraction for this case is done when the rf voltage on the inner wire electrodes of the ion trap is switched OFF, precisely when the amplitude of the rf voltage is zero. The $Rb^+$ ions are loaded into the ion trap using the 473 nm laser from the Rb MOT, held for a short time and then extracted. When the rf is turned OFF the voltages on the extraction electrodes are switched ON simultaneously. In this situation, with the extraction voltages in

our experiment, an asymmetric time of flight (ToF) distribution results, which has a sharp onset and a relatively slower decline. The peak of this ToF distribution is measured to be at $\sim 4.7$ $\mu$s and has a width of $\sim 0.5$ $\mu$s. The ToF signal is illustrated in Fig. 3(a), by the red (solid line) trace. The ion data is collected for a very small ion number per extraction and the signal for 20 cycles is added to obtain the signal shown here.

The histogram in Fig. 3(a) represents the simulated ToF signal for 500 trapped non-interacting ions, with the same voltage conditions imposed. The ions are loaded with an initial gaussian spatial distribution comparable to that of the MOT and a gaussian velocity distribution consistant with the trap depth. The ions are then evolved for 500 rf cycles, and extracted with the specified extraction voltage configuration. The trajectories of two ions which define the two extremes of the ion ToF signal are shown in Fig. 3(b). The acceleration as a function of time, for these two ions as they traverse the extraction potential gradient are shown in Fig. 3(c). In this case the extraction field is stationary in time and hence both the ions experiences the same acceleration at same spatial points. The blue curve (dot-dash) in Fig. 4(a) and 4(b) shows the potential and electric field respectively along the line of extraction at $x = z = 0$.

### *3.2 Atomic Ion: Extraction with rf ON*

The $Rb^+$ ion extraction is performed by switching on the voltages on the extraction electrodes simultaneously, while the trap is operational. The ion arrival time distribution on the CEM from various locations within the ion trap are significantly affected by the phase of the trapping rf field at which the electrodes are switched on. The field along the line of extraction (y axis in this case) is the resultant of the extraction field and the instantaneous trapping rf field. Hence the field at any point along this line varies in time at the rf frequency. The potential and the electric field along the line of extraction for different rf phases is illustrted in Fig. 4(a) and 4(b) respectively. The acceleration of an ion at any given spatial point is determined by the instantaneous field at the point. At the instant when the extraction is switched ON, independent of the phase of the rf, the ions closer to the CEM experience greater acceleration. As the distribution of ions travels towards the CEM, the ion distribution spreads or narrows down as a result of this space and time dependent extraction field. The experimental and simulated arrival time distributions of the extracted ions when the extraction is switched on at different rf phases $\phi$ is shown in Fig 5.

The complexity of ion extraction with the RF fields ON is illustrated in Fig 6, which shows the trajectories of two ions at the extremes of the ToF signal, and the acceleration as a function of time for four selected phases of extraction (a) 0, (b) $\pi/2$, (c) $5\pi/4$ and (d) $7\pi/4$. If the extraction voltages are switched on at phase $\phi = 0$ of the cosine function, as in (a) above, the acceleration experienced by the ion near to the CEM ($\text{ion}_n$) and the

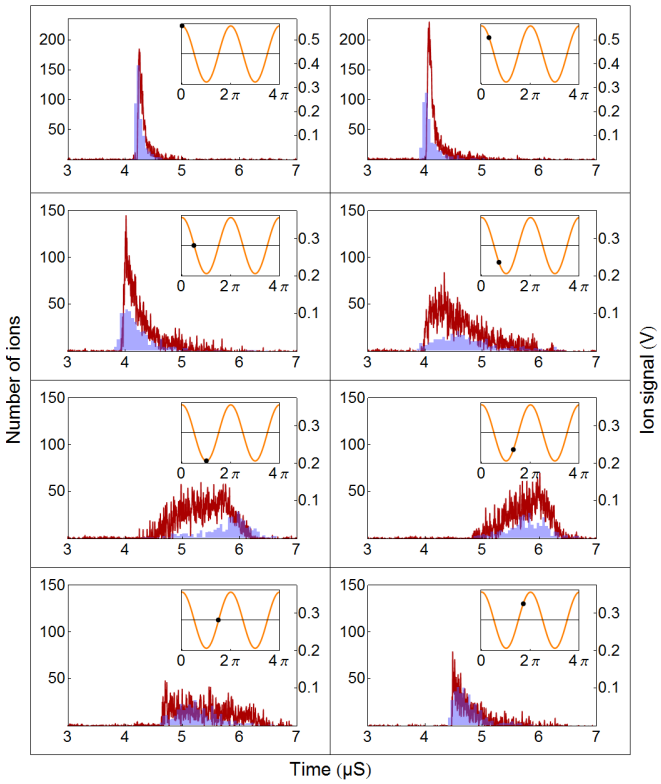


Fig. 5: The ToF signal when the extraction voltage is switched on at different rf phases, $\phi$. The red curve is the experimental signal and the blue histogram is the simulation result. The inset in each figure shows the phase at which the extraction is switched on.

ion away from the CEM ($\text{ion}_f$) is always positive. Hence the velocity is always increased and the average time of flight is 4.3 $\mu$s. The overall acceleration experienced by both the ions are similar and results in a compact arrival time distribution. When the extraction voltages are switched on at phase $\phi = \pi/2$ of the cosine function, the acceleration experienced by the $\text{ion}_n$ is always positive but the $\text{ion}_f$ experiences deceleration at several points along the y axis. As a results, the arrival time distribution of the ions in the cloud spreads. The spread in ion arrival times is very strongly correlated to the phase of the trapping field at the time of switching on the extraction field.

From both experiment and simulations we see that the ToF spread increases as the phase of the cosine changes roughly from $\phi = 0$ to $\pi$ and decreases for phases between $\phi = \pi$ to $2\pi$. When the extraction voltages are switched on at phase $\phi = 5\pi/4$ of Cosine, both the ions experience deceleration at some points along the y axis resulting in an increase in the average time of flight. The deceleration experienced by $\text{ion}_n$ is much more than $\text{ion}_f$ and hence the ion cloud gets spatially focussed and then diverges while travelling along the y axis, giving rise to a spread in ToF signal. The extraction at $\phi = 7\pi/4$ is similar to that of $\phi = 5\pi/4$, but in this case, the amount of deceleration for the two ions as well as the difference in the deceleration between the two ions is less. Hence

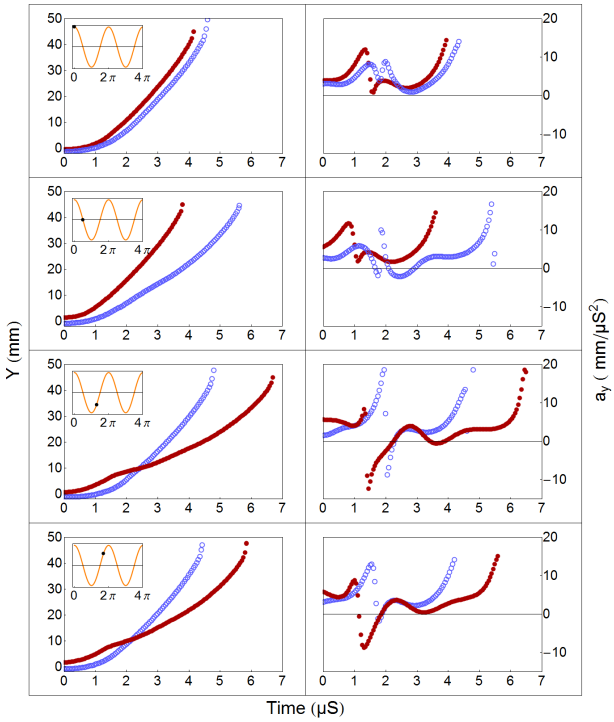


Fig. 6: Figure shows the extracted ion's trajectory from the ion trap center towards the CEM for selected phases of extraction in the left panel. The red(thick) and blue(open) curves represents the trajectory of ions at the two extreme of the ToF signal. The right panel corresponds to the acceleration these ions have experienced as a function of time during their time of flight.

the average ToF and the spread decreases.

When the spread in the ion signal is small, multiple ions reaches the detector within the dead time of the detector, which leads to undercounting of the ions. In Fig. 7, the area under the curve of the ion signal as a function of extraction phase is illustrated. Ion extraction at $\phi \approx \pi$ gives the maximum temporal dispersion and therefore is a more reliable measure of total ion count. Since the ions are extracted in the presence of the rf field, and it takes finite time for the ion to exit the trap volume, the extracted ions see an evolution of the electric field. This evolution of the spatio-temporal electric field during extraction, results in evolving potentials, which alter the arrival times of ions. So when the same number of trapped ions are extracted at different rf phases, the maximum area of the signal peaks just before the $\phi \approx \pi$ value, as seen in Fig. 7.

## 4 Extraction of multiple species of ions

The effect of radial extraction, when multiple species of ions with different masses ($m_1$ and $m_2$) and charge ($e$)are trapped simultaneously, offers another system for a clearer understanding of the method. In a typical mass spectrometer which has uniform extraction fields, when a mixture of ions with same charge $e$, but different masses

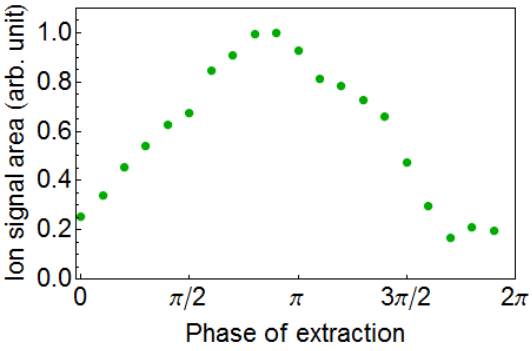


Fig. 7: The normalized area under the curve of the ion signal as a function of phase of extraction, for similar numbers of trapped ions is shown. The area is maximum when the phase of the trap field, at extraction is close to $\phi = \pi$. The slight displacement of the maximum count value is due to the fact that the ions take a finite time to traverse the extent of the trap, and therefore the condition for maximum ion spread is for the case when the ion extraction is marginally advanced from the $\phi = \pi$ instant.

$m_1 < m_2$ are extracted, the ratio between the ToF of the two species is $T_{m2}/T_{m1} = \sqrt{(m_2/m_1)}$. However if the trapping rf is ON during the extraction, as in our case, the ToF of the two masses cannot be related by the above expression, due to the time varying gradient fields. In such a situation the temporal sequence of the ions is significantly altered, a brief study of which is below. Nevertheless it is vital to know that mass spectrometry can be done precisely in this case. This is because in a number of situations when ions and atoms are co-trapped, cold chemistry can easily lead to product ions which need identification. Mass spectrometry offers a general method for such identification. Another aspect is the reliable detection of small numbers of ions of different species, which allows the branching ratios of such processes to be accurately determined.

Here we demonstrate this experimentally as well as by simulation with an example using $Rb^+$ and $Rb_2^+$ ions. The creation fo these ions using the pulsed dye laser has been discussed in section 2. Here we identify $m_1$ with the mass of $Rb^+$ and $m_2 = 2 \times m_1$ as the mass of $Rb_2^+$. The ions are created from the MOT, and extracted from the trap in a manner identical to that for the atomic ion case, after a hold time of 300 $\mu$s. The extraction is done by switching on the extraction voltages at different phases of the rf voltage and the result is shown in Fig 8. In the first panel, the accumulated counts over 4000 ionization and extraction cycles counts of both the ions with rf OFF while extraction is shown. The red curve is the experimental data, the blue and the green histograms are the simulated TOF for $Rb^+$ and $Rb_2^+$ ions respectively. In this case the $T_{m2} = \sqrt{2} \times T_{m1}$, when the times from the extraction to the peak of the detected pulse are considered. The panels 2 to 5 of the Fig 8 show, again the integrated signal for 4000 cycles of the experiment, the ToF distribution for the trapped ions when the extrac-

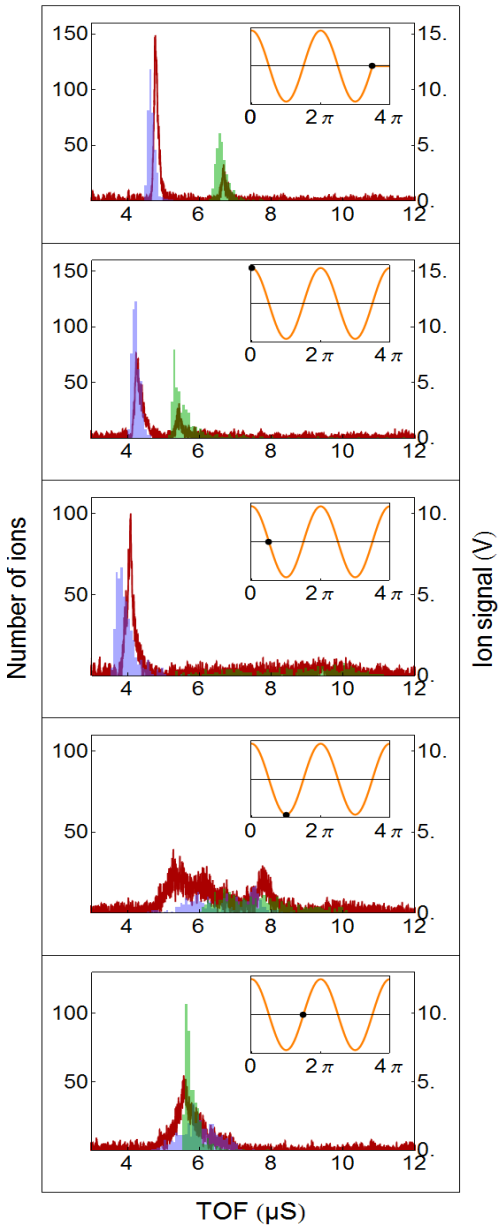


Fig. 8: Panel 1 shows the mass spectrometry of $Rb^+$ and $Rb_2^+$ ions when extracted with rf voltage on the inner wires switched off. The red curves are the experimental data and the blue and green histograms are simulated ToF of $Rb^+$ and $Rb_2^+$ ions respectively. In panels 2 to 5, the time of flight signal of $Rb^+$ and $Rb_2^+$ ions extracted with RF voltage kept ON is shown and the inset indicates the phase at which the extraction voltages are turned ON. The relation $T_{m2} = \sqrt{2} \times T_{m1}$ is satisfied only for the case of rf OFF(panel 1).

tion is switched on at $\phi = 0, \pi/2, \pi$ and $3\pi/2$ of the rf, respectively. At $\phi = 0$, both the ion peaks are distinguishable, but the average ToF as well as the peak seperation is reduced. At $\phi = \pi/2$, $Rb_2^+$ ion signal is spread from $5\mu$S to $11\mu$S but still distinguishable from $Rb^+$ ions. At phases $\phi = \pi$ and $3\pi/2$, $Rb^+$ and $Rb_2^+$ ions signals are merged and cannot be distinguished. In the simulations the distributions of the ion arrival times can be tracked, and this shows that the overlapping spreads of $Rb^+$ and $Rb_2^+$ ions are seen. The merging of ToF of the two ions having mass ratio 2 is because the $Rb_2^+$ ions see a more favourable net acceleration in the extraction compared to the $Rb^+$ ions as a result of the space and time dependent extraction potential. Thus if a mass spectrometric identification is to be made for multiple ion species in the trap, it is necessary to extract the ions with the rf OFF.

Another experimental observation is that for the same CEM voltages, the $Rb_2^+$ ions result in a pulse height distribution with lower heights than the counts registered by the $Rb^+$, when the atomic and molecular ion ToF distributions are well seperated. This can affect the measurement of branching ratios if the counts are integrated to give a spectrum, rather that detected by a pulse counting algorithm.

## 5 Discussion and conclusions

The utility of radial extraction from a compact ion trap design is evident. In the case of single ion species, there is a significant advantage to be had for a more representative count of the trapped ions if the extraction phase is chosen properly. To a certain extent this requirement is imposed by the compact geometry, where the distance between the ion trap and the CEM is of the order of a few cms. A single ion counted by the CEM results in a dead time of $\approx 10$ ns, and this limits the number of ions that can be reliably counted in a single pulse of the extraction to a few $10/\mu$s. Spreading out the ion counts temporally results in a marked improvement in the number of detected ion counts, particularly when the detection is implemented by pulse counting as then the detector pile-up effects are mitigated. The temporal dispersion of trapped ions in extraction is achieved by the choice of rf phase at the time of extraction. In addition the extraction voltage needs to be few times larger than $V_{rf}$, so that all ions are extracted in the first sweep and they do not oscillate in the trap.

Another consequence of the ion extraction with the rf trap ON is that the ion lensing due to the gradients in the fields are not practical to characterize, even in the paraxial limit, because of the time depend potential and the slip in phase while extraction. Nevertheless, explicitly solving the numerical equations of motion for trapped ions gives robust agreement with the experimentally measured ions signals in all the cases discussed here. The extraction which coincides with the turning OFF of the rf trapping field allows the identification of the mass spectrum of multiple species of co-trapped ions. It is possible to improve the resolution for spectroscopy, by increasing the flight time, an improvement that could be implemented with the use of segmented time of flight mass spectrometers [18] without significant loss in the ion counts. In summary, our method controls temporal dispersion beyond the reach of conventional ion ToF mass spectrometry. These techniques will be of great utility in the future studies of trapped ion-neutral mixtures, where

ions arrive in tight bunches, when extracted out of the ion trap.

## Acknowledgements

G. Werth is acknowledged for useful discussions. The authors acknowledge Mr. Narayanaswami and the other members of the RRI machine shop for technically supporting the fabrication of this experiment and Ms. S. Sujatha, RAL, RRI for crucial electronics fabrication.

## References

1. Winthrop W. Smith, Oleg P. Makarov, and Jian Lin. Cold ionneutral collisions in a hybrid trap. *Journal of Modern Optics*, 52(16):2253–2260, 2005.
2. Andrew T. Grier, Marko Cetina, Fedja Oručević, and Vladan Vuletić. Observation of cold collisions between trapped ions and trapped atoms. *Phys. Rev. Lett.*, 102:223201, Jun 2009.
3. Christoph Zipkes, Stefan Palzer, Carlo Sias, and Michael Kohl. A trapped single ion inside a bose-einstein condensate. *Nature*, 464:388–391, 2010.
4. Stefan Schmid, Arne Härter, and Johannes Hecker Denschlag. Dynamics of a cold trapped ion in a bose-einstein condensate. *Phys. Rev. Lett.*, 105:133202, Sep 2010.
5. Wade G. Rellergert, Scott T. Sullivan, Svetlana Kotochigova, Alexander Petrov, Kuang Chen, Steven J. Schowalter, and Eric R. Hudson. Measurement of a large chemical reaction rate between ultracold closed-shell $^{40}$Ca atoms and open-shell $^{174}Yb^{+}$ ions held in a hybrid atom-ion trap. *Phys. Rev. Lett.*, 107:243201, Dec 2011.
6. K. Ravi, Seunghyun Lee, Arijit Sharma, G. Werth, and S.A. Rangwala. Cooling and stabilization by collisions in a mixed ion-atom system. *Nat Commun*, 3:1126, 2012.
7. Felix H. J. Hall and Stefan Willitsch. Millikelvin reactive collisions between sympathetically cooled molecular ions and laser-cooled atoms in an ion-atom hybrid trap. *Phys. Rev. Lett.*, 109:233202, Dec 2012.
8. K. Blaum, Yu. N. Novikov, and G. Werth. Penning traps as a versatile tool for precise experiments in fundamental physics. *Contemporary Physics*, 51(2):149–175, 2010.
9. A. Steane. The ion trap quantum information processor. *Applied Physics B*, 64(6):623–643, 1997.
10. U. Bissbort, D. Cocks, A. Negretti, Z. Idziaszek, T. Calarco, F. Schmidt-Kaler, W. Hofstetter, and R. Gerritsma. Emulating solid-state physics with a hybrid system of ultracold ions and atoms. *Phys. Rev. Lett.*, 111:080501, Aug 2013.
11. Tridib Ray, S. Jyothi, N.Bhargava Ram, and S.A. Rangwala. A thin wire ion trap to study ionatom collisions built within a fabryperot cavity. *Applied Physics B*, 114(1-2):267–273, 2014.
12. S. Jyothi, T. Ray, N. Bhargava Ram, and S. A. Rangwala. Hybrid ion, atom and light trap. *ArXiv e-prints*, December 2013.
13. F. G. Major V. N. Gheorghe and G Werth. *Charged particle traps*. Springer-Verlag Berlin Heidelberg, 2005.
14. M. Holzki. Untersuchung von gekoppelten nichtlinearen oscillationen einer ionenwolke in ionenfallen. Master's thesis, Johannes Gutenberg University, Mainz, 1997.
15. Steven J. Schowalter, Kuang Chen, Wade G. Rellergert, Scott T. Sullivan, and Eric R. Hudson. An integrated ion trap and time-of-flight mass spectrometer for chemical and photo- reaction dynamics studies. *Review of Scientific Instruments*, 83(4):–, 2012.
16. C. Gabbanini, A. Fioretti, A. Lucchesini, S. Gozzini, and M. Mazzoni. Cold rubidium molecules formed in a magneto-optical trap. *Phys. Rev. Lett.*, 84:2814–2817, Mar 2000.
17. A. R. L. Caires, V. A. Nascimento, D. C. J. Rezende, V. S. Bagnato, and L. G. Marcassa. Atomic density and light intensity dependences of the ¡span class="aps-inline-formula"¿¡math display="inline"¿¡msub¿¡mi mathvariant="normal"¿rb¡/mi¿¡mn¿2¡/mn¿¡/msub¿¡/math¿¡/span¿ molecule formation rate constant in a magneto-optical trap. *Phys. Rev. A*, 71:043403, Apr 2005.
18. E Krishnakumar, SVK Kumar, SA Rangwala, and SK Mitra. Excited state dissociative attachment and couplings of electronic states of. *Journal of Physics B: Atomic, Molecular and Optical Physics*, 29:L657, 1996.